View metadata, citation and similar papers at core.ac.uk

brought to you by CORE

provided by Scholarship@Claremont

Claremont Colleges
Scholarship @ Claremont

HMC Senior Theses

HMC Student Scholarship

2011

Simulations of Surfactant Spreading

Jeffrey Wong
Harvey Mudd College

Recommended Citation

Wong, Jeffrey, "Simulations of Surfactant Spreading" (2011). *HMC Senior Theses*. 1.
https://scholarship.claremont.edu/hmc_theses/1

This Open Access Senior Thesis is brought to you for free and open access by the HMC Student Scholarship at Scholarship @ Claremont. It has been accepted for inclusion in HMC Senior Theses by an authorized administrator of Scholarship @ Claremont. For more information, please contact scholarship@cuc.claremont.edu.

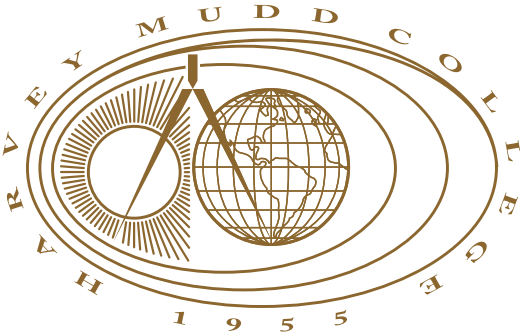

Simulations of Surfactant Spreading

Jeffrey Wong

Rachel Levy, Advisor

Andrew Bernoff, Reader

May, 2011

HARVEY MUDD
COLLEGE
Department of Mathematics

Copyright © 2011 Jeffrey Wong.

The author grants Harvey Mudd College and the Claremont Colleges Library the nonexclusive right to make this work available for noncommercial, educational purposes, provided that this copyright statement appears on the reproduced materials and notice is given that the copying is by permission of the author. To disseminate otherwise or to republish requires written permission from the author.

Abstract

Thin liquid films driven by surface tension gradients are studied in diverse applications, including the spreading of a droplet and fluid flow in the lung. The nonlinear partial differential equations that govern thin films are difficult to solve analytically, and must be approached through numerical simulations. We describe the development of a numerical solver designed to solve a variety of thin film problems in two dimensions. Validation of the solver includes grid refinement studies and comparison to previous results for thin film problems. In addition, we apply the solver to a model of surfactant spreading and make comparisons with theoretical and experimental results.

Contents

List of Figures

Chapter 1

Introduction

A thin film is simply a film of liquid for which the height of the film is small compared to the characteristic length of the problem. The assumption that the film is thin allows significant simplification of the Navier-Stokes equations that govern the film's behavior; through the lubrication approximation an equation for the height of the film can be obtained. The most basic thin film equation is the partial differential equation

$$h_t = -\nabla \cdot \left(\frac{1}{3} h^3 \nabla \nabla^2 h \right). \tag{1.1}$$

Here, the only effect acting on the film are stresses due to the film's curvature. The equation is made more complicated by the introduction of other forces such as gravity and surface tension gradients. The fourth-order term of Equation 1.1 is particularly challenging to solve numerically in more than one dimension. In 2003, Witelski and Bowen proposed an Alternating Direction Implicit (ADI) method for solving the thin film equation efficiently in two dimensions. The application of this method to the thin film equation is relatively new, and continues to be studied. Other methods have been used to solve the equation, such as spectral solvers employed by Warner, Craster, and Matar (2004), but they have been found to generally be less efficient than ADI methods. Complicating the thin film equation with additional terms necessitates semi-implicit methods to handle the parabolic part of the equation (the fourth-order term) implicitly by an ADI method and other terms such as surface-tension gradient effects explicitly.

1.1 Content of the Thesis

The purpose of this work is to develop an open source numerical solver for thin film problems. In particular, we focus on the application of this solver to a problem related to surfactant spreading, but also show how the solver can be adapted to related problems. In Section 1.2 and Section 1.3, the process of surfactant spreading is described as well as the motivating experiment for the application of the numerical solver. In Section 1.4, a derivation of the lubrication model for the surfactant spreading experiment is presented, followed by a discussion of the model. In Chapter 2, the numerical method for solving the equations is described. In Chapter 3, tests of the solver are presented. To verify accuracy, previous work on thin film problems and surfactant spreading are reproduced. To explore efficiency, convergence studies are noted and the required time step is discussed. Chapter 4 contains a discussion of my application of the numerical solver to the model for the motivating surfactant spreading experiment. The numerical results are compared to previous numerics and theory for the equations, as well as to the experimental results. Finally, Chapter 5 summarizes conclusions and describes unanswered questions and directions for future research for both the numerical simulations and modeling of the experiment.

1.2 Thin Liquid Films with Surfactants

Surfactants are chemicals that collect at the surface of a fluid and lower surface tension. Variation in surfactant concentration on the surface produces a surface tension gradient that causes the fluid to flow in order to relieve this stress. Forces on the fluid due to surface tension gradients such as from surfactants are called Marangoni forces. Thin liquid films driven by Marangoni forces have been studied extensively both experimentally and mathematically. Of interest are the spreading dynamics of the film, instabilities such as film rupture and fingering, and the behavior of wave structures that arise as solutions. This process of driving films is relevant to diverse applications, including industrial applications in coating and the effect of surfactants in the lung (Jensen, 1994; Craster and Matar, 2000).

The use of surfactants to provide Marangoni forces provides an added complication compared to, for instance, a temperature gradient, because the surfactant is carried with the fluid. Insoluble surfactant lies entirely on the surface and so is transported at the surface velocity of the fluid, but

soluble surfactant can exist in part in the bulk of the fluid. Surfactants have hydrophobic tails and hydrophilic heads, and so beyond a sufficient concentration (the critical micelle concentration, or CMC) even an insoluble surfactant can organize into micelles, structures where the within the bulk of the fluid surfactant molecules are arranged with hydrophilic head outward and the hydrophobic tail inside. The transfer of surfactant between these states, and to the interface of the fluid leads to interesting dynamics (Edmonstone et al., 2006).

In this work a standard lubrication model for insoluble surfactant spreading is considered, which is a system of fourth-order partial differential equations for the film height and surfactant concentration. Similarity solutions have provided theoretical descriptions of spreading rates, such as those described by Jensen (1994). The system includes forces and parameters that affect solutions, which include the fourth-order capillary effects, Marangoni forces, surface diffusion of the surfactant, and gravity-driven spreading of the film. The fourth-order terms allow for fingering instabilities to occur in the system, which are a rich area of study; the mechanism for fingering in the system is quite complicated and not fully understood. Numerical methods have been developed that appear to be reasonably effective in computing solutions to these equations, for which the numerical difficulties are significant (Warner et al., 2004; Witelski and Bowen, 2003).

1.3 Experiment for Surfactant Spreading

In the experiment relevant to this work, surfactant is deposited on a thin film of glycerin, typically with a height on the order of a millimeter. The surfactant is initially dissolved in chloroform, and its tail includes a fluorescent tag that is used to image the surfactant concentration during the experiment (Fallest et al., 2010). There are two configurations for this experiment: a disk of surfactant or the opposite case in which surfactant is placed outside that disk (an "anti-disk"). A metal ring is used to contain the surfactant while it is being deposited and the chloroform is allowed to evaporate, which is then lifted and the system allowed to evolve. In both cases the initial surfactant profile is intended to be axisymmetric, and this symmetry holds reasonably well as spreading occurs.

This work is motivated by the surprising result for an anti-disk that demonstrates experimentally that the surfactant profile is static (Allison et al., 2010). Interestingly, in the case of a disk of surfactant spreading, directed radially outward, does occur. The lack of spreading is contrary

to the theoretical results such as those of Jensen (1994) and suggest that the experiment may require greater resolution or the model may not be an accurate reflection of our experimental system.

1.4 Derivation of the Model

The following derivation of the lubrication model largely follows that in Peterson (2010). Consider a thin film of liquid on a horizontal plane. Let $\mathbf{v} = (u, v, w)$ be the velocity field within the fluid in three dimensions and let $\mathbf{u} = (u, v)$ be the projection of that velocity onto the x, y plane. Let $p(x, y, z)$ be the pressure in the fluid, and let $h(x, y, t)$ be the height of the free surface. Let $\Gamma(x, y, t)$ be the surfactant concentration on the surface of the fluid. Finally, let σ be the surface tension of the film. The surface tension depends only on the concentration of surfactant on the surface, so we write $\sigma = \sigma(\Gamma)$, which is the equation of state for surface tension. Denote dimensionless quantities with a hat, and define scalings

$$u = U\hat{u}, \qquad w = W\hat{w}, \qquad x = L\hat{x}, \qquad z = H\hat{z}. \tag{1.2}$$

Also assume that the scale for length and velocity in the x-direction and y-direction are the same; that is, $v = U\hat{v}$ and $y = L\hat{y}$. The fluid is assumed to be incompressible and the Reynolds number $Re = \frac{\rho LU}{\mu}$ is assumed to be small, so the fluid is described by the Stokes equations

$$0 = -\nabla p + \mu \nabla^2 \mathbf{v}, \tag{1.3}$$

$$0 = \nabla \cdot \mathbf{v}, \tag{1.4}$$

where μ is the fluid viscosity. To apply the lubrication approximation, the assumption is made the film is very thin, so the aspect ratio $\epsilon = H/L$ is small.

1.4.1 Nondimensionializing the Stokes Equations

The assumption that $\epsilon \ll 1$ allows for significant simplification of the Stokes equations by neglecting small terms that arise in the nondimensionalization. To nondimensionalize the equations, first note that balancing scales exactly in Equation 1.4 gives the scaling

$$w = \epsilon U \hat{w}$$

for the vertical velocity. Equation 1.3, rewritten in terms of these scales and dimensionless quantities, becomes the system

$$\begin{aligned} \epsilon H p_{\hat{x}} &= \mu\left(\epsilon^2 U(\hat{u}_{\hat{x}\hat{x}} + \hat{u}_{\hat{y}\hat{y}}) + U\hat{u}_{\hat{z}\hat{z}}\right) && (1.5)\\ \epsilon H p_{\hat{y}} &= \mu\left(\epsilon^2 U(\hat{v}_{\hat{x}\hat{x}} + \hat{v}_{\hat{y}\hat{y}}) + U\hat{v}_{\hat{z}\hat{z}}\right) && (1.6)\\ H P_{\hat{z}} &= \mu(\epsilon^3 U(\hat{w}_{\hat{x}\hat{x}} + \hat{w}_{\hat{y}\hat{y}}) + \epsilon U\hat{w}_{\hat{z}\hat{z}}) - H^2\rho g. && (1.7) \end{aligned}$$

Balancing the left hand side of Equation 1.5 with the term $\mu U\hat{u}_{\hat{z}\hat{z}}$ gives the pressure scale

$$p = p_0\hat{p}, \qquad p_0 = \frac{\mu U}{\epsilon H}.$$

Applying the pressure scaling and retaining only terms of at most order ϵ in Equations 1.5, 1.6, and 1.7 gives the system (in dimensional form)

$$\begin{aligned} p_x &= \mu u_{zz} && (1.8)\\ p_y &= \mu v_{zz} && (1.9)\\ p_z &= -\rho g. && (1.10) \end{aligned}$$

1.4.2 Boundary Conditions

At the surface of the film, a stress balance must be satisfied. Let n be an outward normal to the surface $h(x, y)$. Let T_{air} and T_f be the stress tensors for the air above the fluid, and the fluid itself, respectively. The force by the fluid on the air at the surface is $(-n) \cdot T_f$ and the force by the air on the fluid is $n \cdot T_{air}$. These force are balanced by effects due to the curvature of the film in the normal direction and the Marangoni force in the tangential direction, which leads to the balance

$$n \cdot T_{air} - n \cdot T_f = (\gamma \nabla_s \cdot n)n + \nabla_s\sigma. \tag{1.11}$$

The gradient operator ∇_s in Equation 1.11 is a surface gradient. However, by the lubrication approximation, the film is approximately flat and so the surface gradient can be replaced by the usual gradient. The stress tensor for a viscous, Newtonian fluid is

$$T_f = -pI + \mu(\nabla u + \nabla u^T).$$

The stress tensor for the air is taken simply to be

$$T_{air} = -p_{atm}I$$

as the viscosity of the air is negligible compared to that of the fluid.

Normal stress

Dotting the stress balance of Equation 1.11 with n gives

$$p - p_{atm} - 2w_z = \gamma \nabla \cdot n, \qquad \text{at } z = h, \tag{1.12}$$

where $\nabla \cdot n$ is twice the mean curvature of the free surface h, γ is a surface tension parameter and p_{atm} is the atmospheric pressure. The term w_z is small relative to the curvature term so long as the capillary number is small, so it is neglected. Explicitly, $\nabla \cdot n$ is given by

$$\nabla \cdot n = -\frac{h_{xx} + h_{yy} + h_x^2 h_{yy} + h_y^2 h_{xx} - 2h_x h_y h_{xy}}{(1 + h_x^2 + h_y^2)^{3/2}}. \tag{1.13}$$

Because $h_x \sim H/L = \epsilon$ and $h_y \sim \epsilon$, the denominator can be expanded using the binomial approximation as

$$(1 + h_x^2 + h_y^2)^{-3/2} \approx 1 - \frac{3}{2}(h_x^2 + h_y^2) + \cdots = 1 + O(\epsilon).$$

In the numerator, h_{xx} and h_{yy} are of order ϵ^2, whereas all other terms are of higher order. Hence Equation 1.12 becomes

$$p - p_{atm} = -\gamma \nabla^2 h \tag{1.14}$$

by retaining terms up to ϵ^2.

Tangential Stress

Dotting Equation 1.11 with a tangent vector t to the surface gives

$$0 = n \cdot T \cdot t + \nabla \sigma \cdot t \tag{1.15}$$

Because h_x, h_y are of order ϵ in the lubrication approximation, the normal is $n = (0, 0, 1)$ and the tangent vectors are horizontal. Equation 1.15 then simplifies to the system

$$\sigma_x = \mu(u_z + w_x), \qquad \sigma_y = \mu(v_z + w_y).$$

Applying the lubrication approximation again shows that w_x and w_y are small and can be neglected, yielding the final condition

$$\sigma_x = \mu u_z, \qquad \sigma_y = \mu v_z, \qquad \text{at } z = h. \tag{1.16}$$

No Slip

Finally, the no slip condition is imposed at the bottom surface of the fluid:

$$u = v = 0, \qquad \text{at } z = 0. \tag{1.17}$$

1.4.3 Solving for u

Recall that $\mathbf{u} = (u, v)$, defined in the $x - y$ plane. The other component, w, of the full velocity $\mathbf{v}$is not used further in the derivation. By Equation 1.10, the pressure p is linear in z and so applying the normal stress condition of Equation 1.14 gives

$$p = \rho g(h - z) + p_{atm} - \gamma \nabla^2 h. \tag{1.18}$$

Differentiating with respect to x and y gives

$$p_x = \rho g h_x - \gamma (\nabla^2 h)_x, \tag{1.19}$$
$$p_y = \rho g h_y - \gamma (\nabla^2 h)_y. \tag{1.20}$$

Equating this with the expressions for p_x and p_y in Equations 1.8 and 1.9 eliminates the pressure variable, yielding

$$\mu \frac{\partial^2 \mathbf{u}}{\partial z^2} = \rho g \nabla h - \gamma \nabla \nabla^2 h. \tag{1.21}$$

Integrating Equation 1.21 twice with respect to z, and applying the tangential stress balance in Equation 1.16 and the no slip condition 1.17 gives the velocity profile,

$$\mathbf{u} = \frac{1}{\mu} \left(\rho g \nabla h - \gamma \nabla \nabla^2 h \right) \left(\frac{1}{2} z^2 - hz \right) + \frac{1}{\mu} \nabla \sigma z. \tag{1.22}$$

1.4.4 Conservation

Let $\bar{\mathbf{u}}$ be a depth averaged velocity in the $x - y$ plane, computed from Equation 1.22 as

$$\bar{\mathbf{u}} = \frac{1}{h} \int_0^h \mathbf{u} dz \tag{1.23}$$
$$= \frac{1}{h\mu} \left(- \left(\rho g \nabla h - \gamma \nabla \nabla^2 h \right) \frac{1}{3} h^3 + \frac{1}{2} h^2 \nabla \sigma \right). \tag{1.24}$$

Consider a column of fluid over an area S in the $x-y$ plane. Conservation of the fluid implies that

$$\frac{d}{dt}\iint_S h dA = -\int_{\partial S}(h\bar{\mathbf{u}})\cdot d\hat{n} = -\iint_S \nabla\cdot(h\bar{\mathbf{u}})dA$$

via an application of the divergence theorem, where $h\bar{\mathbf{u}}$ is the fluid flux, using the depth-averaged velocity, and n is an outward normal to ∂S. The area S is arbitrary, so conservation in differential form is an equation for the film height,

$$h_t + \nabla\cdot(h\bar{\mathbf{u}}) = 0. \tag{1.25}$$

The surfactant is transported along the surface of the fluid at the surface velocity, obtained by setting $z = h$ in Equation 1.22,

$$\mathbf{u_h} = -\frac{1}{\mu}\left(\rho g\nabla h - \gamma\nabla\nabla^2 h\right)\left(\frac{1}{2}h^2\right) + \frac{1}{\mu}\nabla\sigma h. \tag{1.26}$$

The surfactant also diffuses according to Fick's law, which results in the surfactant evolution equation

$$\Gamma_t + \nabla\cdot(\Gamma\bar{\mathbf{u}}_\mathbf{h}) = D\nabla^2\Gamma \tag{1.27}$$

where D is the surface diffusivity.

Nondimensional Equations

In addition to the scalings in Equation 1.2, define scalings $\sigma = S\hat{\sigma}$ for surface tension and $t = T\hat{t}$ for time. Rewriting Equation 1.25 in terms of nondimensional quantities and multiplying through by T/H gives

$$\hat{h}_{\hat{t}} + \frac{HTS}{\mu L^2}\nabla\cdot(\frac{1}{2}\hat{h}^2\nabla\sigma) = \frac{TH^3\rho g}{\mu L^2}\nabla\cdot(\frac{1}{3}\hat{h}^3\nabla\hat{h}) - \frac{TH^3}{\mu L^4}\nabla\cdot(\frac{1}{3}\hat{h}^3\nabla\nabla^2\hat{h}). \tag{1.28}$$

To make the coefficient of the Marangoni term unity, the time scale is defined to be $T = \frac{\mu L^2}{SH}$. Defining nondimensional coefficients

$$\beta = \frac{\rho g H^2}{S}, \qquad \kappa = \frac{\gamma H^2}{SL^2}, \qquad \delta = \frac{\mu D}{SH}, \tag{1.29}$$

yields the nondimensionalized equations (with the hats omitted)

$$h_t + \nabla\cdot(\frac{1}{2}h^2\nabla\sigma) = \beta\nabla\cdot(\frac{1}{3}h^3\nabla h) - \kappa\nabla\cdot(\frac{1}{3}h^3\nabla\nabla^2 h) \tag{1.30}$$

for the film height and

$$\Gamma_t + \nabla \cdot (h\Gamma\nabla\sigma) = \beta\nabla \cdot (\frac{1}{2}h^2\Gamma\nabla h) - \kappa\nabla \cdot (\frac{1}{2}h^2\Gamma\nabla\nabla^2 h) + \delta\nabla^2\Gamma. \quad (1.31)$$

for the surfactant.

1.5 Description of the Model

The nondimensionalized coefficients in Equations 1.30 and 1.31 describe the strength of the various forces acting on the film relative to the Marangoni forces. The second-order β term describes gravity-driven spreading of the film. The fourth-order κ term describes capillary effects in the film. The function $\sigma(\Gamma)$ is the equation of state that describes the reduction in surface tension of the film by the surfactant. Hence the $\nabla\sigma$ term describes Marangoni forces dues to the surfactant, which drives the system. Finally, the δ term describes surface diffusion of the surfactant, which is usually small.

1.5.1 Dimensionless Quantities

The values of the characteristic scales are as follows in the experiment. The length scale $L = 0.8\ cm$ is the radius of the ring containing the surfactant. The height scale $H = 0.098$ cm is the initial film thickness. The surface tension scale $S = 27.9$ dyne/cm is given by $\sigma_0 - \sigma_m$ where $\sigma_0 = \gamma$ is the glycerin surface tension without surfactant and σ_m is the surface tension when the surface is entirely contaminated by surfactant. The computed time scale is $T \approx 0.5$ s.

Values for physical quantities are as follows: $\rho \approx 1.26$ g/cm^3 is the fluid density; $g = 980$ cm/s^2 is the acceleration of gravity; $\sigma_0 = 63.4$ dyne/cm, $\mu \approx 8.3$ g/cm $\cdot$ s is the dynamic viscosity; and $D \approx 10^{-4}$ cm^2/s is the surface diffusion parameter. The nondimensional coefficients (Equation 1.29) have values

$$\beta = 0.271, \qquad \kappa = 0.013, \qquad \delta = 3 \times 10^{-5}. \quad (1.32)$$

Other nondimensional values of note include the Reynolds number, which depends on the horizontal velocity scale U. The velocity scale U is obtained from Equation 1.21 by balancing dimensions in the first two terms to give $U = \frac{\rho g H^3}{\mu L} \approx 1.01$ cm/min and so the Reynolds number is

$$Re = \frac{\rho L U}{\mu} = \frac{\rho^2 g H^3}{\mu^2} \approx 0.02.$$

1.5.2 Initial/Boundary Conditions

Initial conditions for outward spreading are chosen to represent a deposit of some number m of monolayers of surfactant within a disk of (nondimensionalized) radius 1. For axisymmetric outward spreading, this initial condition takes the form

$$h(r,0) = 1, \qquad \Gamma(r,0) = \begin{cases} m(1-r)^{10} & \text{if } r < 1 \\ 0 & \text{if } r > 1, \end{cases} \tag{1.33}$$

where m is the number of monolayers of surfactant used. The initial condition for inward spreading is similarly taken to be

$$h(r,0) = 1, \qquad \Gamma(r,0) = \begin{cases} mr^{10} & \text{if } r < 1 \\ m & \text{if } r > 1. \end{cases} \tag{1.34}$$

In experiments, the initial height profile is actually nonconstant due to the meniscus that forms when the metal ring bounding the surfactant is lifted. The initial film height can be modified to be

$$h(r,0) = \begin{cases} a\sin(2r - \pi/3) + (1+a) & r < 11\pi/12 \\ 1 & \text{otherwise,} \end{cases} \tag{1.35}$$

where $a \approx 0.15$ describes the amplitude of the meniscus. The effect of the meniscus has not been explored in this work.

1.5.3 Equations of State

The equation of state describes the influence of the surfactant on the surface tension of the film. By convention, $\Gamma = 1$ corresponds to a monolayer of surfactant, which is the amount of surfactant required for the film surface tension to be lowered to σ_m, the contaminated surface tension used in the nondimensionalization. The function $\sigma(\Gamma)$ must also satisfy $\sigma'(\Gamma) \leq 0$ since surfactants lower surface tension. Although usually σ' is strictly negative, in some proposed equations of state there is a Γ_c (usually 1) beyond which $\sigma'(\Gamma) = 0$ for $\Gamma \geq \Gamma_c$, which represents saturation of the surfactant once it achieves a monolayer on the fluid surface.

Experiments have been performed to determine the equation of state experimentally (Bull and Grotberg, 2003). A variety of models have been proposed, and there is no clear indication of which equation is appropriate.

The simplest, and most mathematically convenient equation of state is the linear equation

$$\sigma(\Gamma) = 1 - \Gamma$$

which provides qualitatively reasonable results in surprisingly many cases, although its behavior is not suitable for $\Gamma > 1$. A limiting behavior of $\Gamma^{-1/3}$ as $\Gamma \to \infty$ is proposed by Sheludko and reflected in the Langmuir equation of state, which is given by

$$\sigma(\Gamma) = \frac{\alpha + 1}{(1 - ([1 + 1/\alpha]^{1/3} - 1)\,\Gamma)^3}. \tag{1.36}$$

Here, α is a constant the controls the linearity of the equation of state, which is approximately linear in the limit $\alpha \to \infty$ (Warner et al., 2004). Like the linear equation of state, the Langmuir equation is valid only for monolayer flow (Warner et al., 2004). For the most part, the family of (reasonable) equations of state with $\sigma' < 0$ produces the same qualitative behavior for a wide variety of cases, including fingering phenomena (Warner et al., 2004), so long as $\Gamma < 1$.

In order to account for multiple layers of surfactant, Grotberg proposed the multilayer equation of state

$$\sigma(\Gamma) = \frac{1}{(1 + \mu\Gamma)^3}, \tag{1.37}$$

for which $\sigma'(\Gamma) \to 0$ as $\Gamma \to 0$, although σ' is never exactly 0 (Borgas and Grotberg, 1988). This approximates the notion of saturation of surfactant at a monolayer. To achieve saturation precisely, I have chosen to consider a simple model given by

$$\sigma(\Gamma) = \begin{cases} (1 - \Gamma)^3 & \Gamma < 1 \\ 0 & \Gamma > 1 \end{cases}. \tag{1.38}$$

which is mentioned in (Borgas and Grotberg, 1988) with respect to equations of state for diffusion, but not for surface tension. When the equation of state has $\sigma'(\Gamma) = 0$, there is possibly a degeneracy introduced into Equation 1.31, suggesting the possibility of qualitatively distinct behavior for Equation 1.38 compared with Equation 1.36.

Chapter 2

Numerical Method

The numerical solver, designed by Jonathan Claridge (at the University of Washington), is intended to efficiently solve thin film problems in two dimensions (2011). The solver uses a finite-volume method to ensure conservation. For a finite-volume method, the computational domain is partitioned into cells and the average over a cell of the dependent variable is considered. Given that the quantity is conserved, the cell average can be updated by considering the fluxes into the cell. By updating cells by adding fluxes, the method is ensured to be conservative so long as there is no flux at the boundary. The equations are first split into two parts, hyperbolic and parabolic, and each is solved using a method specific to that kind of problem. For the hyperbolic system, the CLAWPACK (Conservation LAWs PACKage) software package is employed to solve the equations Leveque and Berger (2010). CLAWPACK provides a convenient framework for solving hyperbolic problems in a conservative way (the details of which are in the following section), using finite-volume methods, as well as providing plotting tools for the resulting data.

For the parabolic system, we use an Alternating Direction Implicit (ADI) method to solve the system in two dimensions. The method is based on the ADI method for solving the thin film equation proposed by Witelski and Bowen (2003). ADI methods have been shown to be effective at computing two-dimensional solutions to the thin film equation, including the system in question here. Other methods, such as spectral solvers, have been used but tend to be less efficient (Warner et al., 2004). The concept of the ADI method is to split the two-dimensional PDE into parts that act only in one dimension, which must be done through careful approximation in particular because of the cross-terms (e.g., h_{xxyy}) that arise in the fourth-order

term of the film equation. Splitting by dimension in this way allows for great efficiency in computation.

The film and surfactant equations are assumed to act independently, so each is solved separately at each step. Splitting between the hyperbolic and parabolic terms is handled using Godunov splitting, for which alternating steps in time are taken for each part. This splitting method is first-order in time.

2.1 Setup for the Solver

The computational domain is taken to be a rectangle $[x_l, x_r] \times [y_l, y_r]$ which is usually square (but does not have to be). Let m be the number of cells in the x direction, and let n be the number of cells in the y direction. For convenience, let $x_i = x_l + (i - 1/2)\Delta x$ and $y_j = y_l + (j - 1/2)\Delta y$. This domain is partitioned into cells of width Δx and height Δy, where the cell centers are at (x_i, y_j) with $1 \leq i \leq m$ and $1 \leq j \leq n$. While cells outside this range of indices are not the domain, values for quantities in these cells are necessary for the solver and are determined by boundary conditions. Each cell has four interfaces, which are noted with half-points in one coordinate; for example, $(x_{i+1/2}, y_j)$ for the right interface of the (i, j) cell. A diagram of cells is shown in Figure 2.1.

Boundary Conditions No flux conditions are imposed on all boundaries. The no flux conditions for the system require that the flux is zero for both equations on the boundary, so for a normal $\hat{n}$ to the interface,

$$\nabla h \cdot \hat{n} = 0, \qquad \nabla \nabla^2 h \cdot \hat{n} = 0, \qquad \nabla \Gamma \cdot \hat{n} = 0.$$

Values for h, Γ and their derivatives for cells outside the domain can are constructed by either even or odd extension of the data across the boundary as appropriate. For example, the condition $\nabla h = 0$ in Equation 2.1 requires that $h_x = 0$ on the left boundary of the domain, so the data can be extended using the even extension $h(x_i, y_j) = h(x_{-i}, y_j)$. Similarly, $\Gamma_x = 0$ on that edge so the data for Γ is extended in the same way.

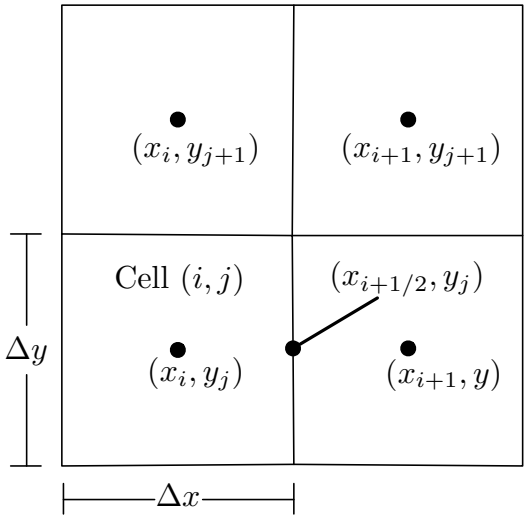

Figure 2.1 Diagram of the computational domain, shown near the cell centered at (x_i, y_j).

2.2 Hyperbolic Terms

The hyperbolic terms of the surfactant spreading Equations 1.30 and 1.31 are

$$0 = h_t + \nabla \cdot \left(\frac{1}{2} h^2 \nabla \sigma \right) \tag{2.1}$$

$$0 = \Gamma_t + \nabla \cdot \left(\frac{1}{2} h^2 \Gamma \left(\kappa \nabla \nabla^2 h - \beta \nabla h \right) \right). \tag{2.2}$$

The hyperbolic terms of the equation are solved using the CLAWPACK software package for finite-volume hyperbolic problems. The motivation for the method is as follows. Because the value of the dependent variable in a cell is represented by its average, the data is piecewise constant. Thus, to determine the flux across an interface, a Riemann problem must be solved at that interface. A Riemann problem refers to a conservative partial differential equation with initial data that is piecewise constant with a single discontinuity. Because of the simple initial condition, the Riemann problem is tractable to solve. Once data is obtained from the Riemann solutions at the interfaces, the cells can be updated.

There are two Riemann solvers specified for each problem, a normal solver to update fluxes normal to cell interfaces and a transverse solver to correct for abnormal flux. The normal Riemann solver acts on a one-dimensional slice of the data, and solves the Riemann problem across an interface, with the value on either side given by the cell averages. The notation used in this section follows that in Leveque (2002). In particular, there are four quantities required for the normal Riemann solver. Let $(i+1/2, j)$ denote a value on the interface between the cells (i, j) and $(i+1, j)$ and consider the Riemann solution normal to that interface. Let $s_{i+1/2,j}$ be the speed of the relevant wave in that solution, and let $Z_{i+1/2,j}$ be the difference in flux for that solution. Finally, the flux difference $Z_{i+1/2,j}$ is split into its right and left-going parts, $A^+_{i+1/2,j}$ and $A^-_{i+1/2,j}$, so that $Z_{i+1/2,j} = A^+_{i+1/2,j} + A^-_{i+1/2,j}$. For a horizontal one-dimensional slice, suppress the index j. At a horizontal interface $(i, j+1/2)$, let $Z_{i,j+1/2}$ be the difference in flux for the (vertical) solution. Also, denote by $B^{\pm}_{i,j+1/2}$ be the corresponding up-going and down-going fluxes at that interface. These are the quantities that must be found from the Riemann solution and supplied to CLAWPACK.

2.2.1 Normal Riemann Solver

The hyperbolic term of the film-height equation Equation 2.1 is a spatially-varying Burgers-like advection. As the hyperbolic terms of the surfactant equation are similar, the solver will be described here in detail only for the film height equation. Consider a Riemann problem for a one-dimensional slice of the equation in the x-direction between the i-th and $(i+1)$st cells, with the interface at $x_{i+1/2}$. Let u_i, u_{i+1} be approximations to σ_x in the respective cells (computed via central differencing) and let $f_i(h) = \frac{1}{2}h^2 u_i$ be the flux function in cell i. The relevant equation is

$$0 = \begin{cases} h_t + (f_i(h))_x & x < x_{i+1/2} \\ h_t + (f_{i+1}(h))_x & x > x_{i+1/2}, \end{cases} \tag{2.3}$$

with Riemann initial data

$$h(x) = \begin{cases} h_i & x < x_{i+1/2} \\ h_{i+1} & x > x_{i+1/2}, \end{cases} \tag{2.4}$$

where h_i, h_{i+1} are the film height values in their respective cells. The appropriate solution to use for this Riemann problem depends on the sign of the values u_i and u_{i+1}. Suppose u_{i-1} and u_i are both positive. Then the

Riemann solution consists of two waves: a stationary wave at the interface connecting h_i to an intermediate state h^*, and a right-going wave connecting h^* to h^{i+1}. A diagram of the solution is shown in Figure 2.2. The stationary wave has speed 0 and so, according to the Rankine-Hugoniot condition, h^* can be found from the relation

$$f_{i+1}(h^*) = f_i(h_i).$$

The flux difference is given simply by

$$Z_{i+1/2} = f_{i+1}(h_{i+1}) - f_i(h_i). \tag{2.5}$$

For the right-going wave, the Rankine-Hugoniot condition gives the speed as

$$s_{i+1/2} = \frac{f_{i+1}(h_{i+1}) - f_i(h^*)}{h_{i+1} - h^*} \tag{2.6}$$

and the fluctuations are set to

$$A^+_{i+1/2} = Z_{i+1/2}, \qquad A^-_{i+1/2} = 0.$$

The assignment for a left-going wave is analogous to the right-going case. If, however, u_i and u_{i+1} have opposite signs then there is no movement across the interface and so $s_{i+1/2} = 0$. The value of $Z_{i+1/2}$ in this case is taken to be zero, although it has no effect on the update formula because that term will be multiplied by the speed and so will vanish. Here, in order to conserve mass the fluctuations are set to

$$A^+_{i+1/2} = -f_i(h_i), \qquad A^-_{i+1/2} = f_{i+1}(h_{i+1}).$$

2.2.2 Transverse Riemann Solver

The transverse solver determines correction fluxes that correspond to flux not normal to an interface, which are used to improve the accuracy of the solver. Given an interface $(i + 1/2, j)$ and fluctuation $A^+_{i+1/2,j}$, split this fluctuation into two parts: a flux $B^+A^+_{i+1/2,j}$ that influences the interface $(i + 1, j + 1/2)$, and a flux $B^-A^+_{i+1/2,j}$ that influences the interface $(i + 1, j - 1/2)$. Similarly, let $B^\pm A^-_{i-1/2,j}$ be parts of $A^-_{i-1/2,j}$ that influence the interfaces $(i - 1, j \pm 1/2)$. A diagram of the transverse fluxes is shown in Figure 2.3.

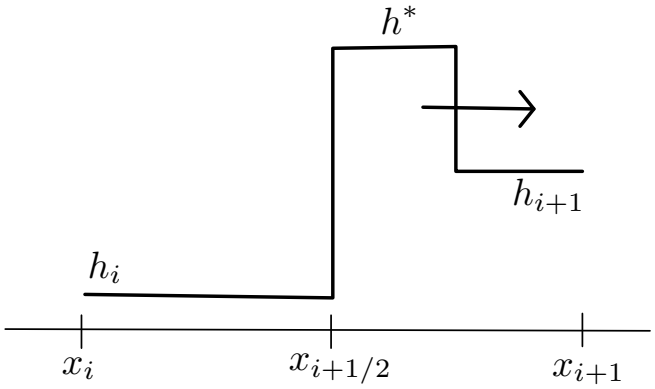

Figure 2.2 Riemann solution for the problem at the interface $x_{i+1/2}$ when the speeds u_i, u_{i+1} in corresponding cells are both positive. The solution has a stationary wave at the interface and a right-moving wave.

The value of the fluctuation is obtained by approximating the vertical velocity for the wave and multiplying that by $A^{\pm}_{i+1/2,j}$. For instance, consider $B^+A^-_{i+1/2,j}$. For the film height the flux is $f(h) = \frac{1}{2}h^2\nabla\sigma$ and so the vertical velocity is approximately $f'(h) = h\sigma_y$, with the value of σ_y used being its value in the cell (i, j) and h approximated by averaging the two heights of the piecewise constant wave in that cell. As with the normal solver, if σ_y changes sign across the interface $(i, j + 1/2)$ the wave crosses the transverse fluctuation is set to 0.

2.2.3 Updating the Cell Values

The cells are updated by a wave propagation method using the fluxes obtained from the normal and transverse solvers:

$$\begin{aligned} q^{n+1}_{i,j} &= q_{i,j} - \frac{\Delta t}{\Delta x}\left(A^+_{i-1/2,j} + A^-_{i+1/2,j}\right) - \frac{\Delta t}{\Delta y}\left(B^+_{i,j-1/2} + B^-_{i,j+1/2}\right) \\ &- \frac{\Delta t}{\Delta x}\left(F_{i+1/2,j} - F_{i-1/2,j}\right) - \frac{\Delta t}{\Delta y}\left(G_{i,j+1/2} - G_{i,j-1/2}\right). \end{aligned}$$

The last two terms are for correction fluxes $F_{i-1/2,j}$ at each interface between the cells for $q_{i-1,j}$ and $q_{i,j}$ and correction fluxes $G_{i,j-1/2}$ for the interfaces between $q_{i,j-1}$ and $q_{i,j}$. The addition of correction fluxes makes the method second order and improves its accuracy. The Riemann solution from the

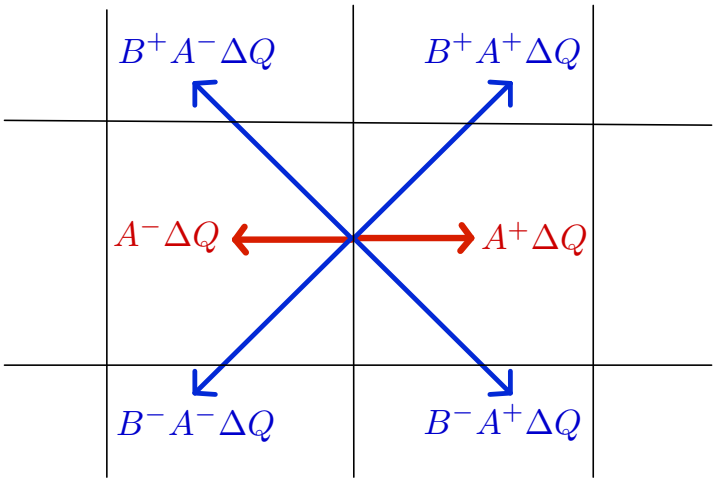

Figure 2.3 Transverse fluxes at a vertical interface. The transverse fluxes are shown in blue and the normal, horizontal fluxes are shown in red.

normal solver from the horizontal solves are used to update $F_{i-1/2,j}$ as

$$F_{i-1/2,j} = \frac{1}{2}\text{sgn}(s_{i-1/2,j})\left(1 - \frac{\Delta t}{\Delta x}|s_{i-1/2,j}|\right)\tilde{Z}_{i-1/2,j}, \tag{2.7}$$

where $\tilde{Z}$ is the flux wave Z with a limiter applied. The limiter used here is the MC limiter $\phi(\theta) = \max(0, \min(\frac{1}{2}(1+\theta), 2, 2\theta))$. The limited wave is defined by

$$\tilde{Z}_{i+1/2,j} = Z_{i+1/2,j}\phi(Z_{I+1/2,j}/Z_{i+1/2,j}),$$

where I is $i+1$ if the wave moves to the right and $i-1$ otherwise (it is the index for the nearest upwind interface). The ratio that is the argument of the limiter reflects the smoothness of the data, so the limiter "limits" the wave when that ratio becomes large.

The other contribution to F is from the transverse fluctuations $A^{\pm}B^{\pm}_{i,j-1/2}$ obtained from the transverse solver applied to the vertical fluxes $B^{\pm}_{i,j-1/2}$. F is further updated by the influence of these transverse fluxes as

$$\begin{aligned} F_{i-1/2,j} := F_{i-1/2,j} &- \frac{\Delta t}{2\Delta x}B^+A^+_{i-1,j-1/2} - \frac{\Delta t}{2\Delta x}B^-A^+_{i-1,j+1/2} \\ &- \frac{\Delta t}{2\Delta x}B^+A^-_{i,j-1/2} - \frac{\Delta t}{2\Delta x}B^-A^-_{i,j+1/2}. \end{aligned}$$

The same process, except using the normal fluxes obtained from vertical solves and transverse fluxes from horizontal solves, is used to update $G_{i,j-1/2}$.

2.3 Parabolic Terms

The parabolic parts of the surfactant-spreading equations Equation 1.30 and Equation 1.31 are

$$0 = h_t + \nabla \cdot \left(\frac{1}{3} h^3 \left(-\beta \nabla h + \kappa \nabla \nabla^2 h \right) \right), \tag{2.8}$$

$$0 = \Gamma_t + \nabla \cdot \left(h \Gamma \nabla \sigma \right). \tag{2.9}$$

The parabolic terms (most notably the fourth-order terms in the film height equation) are solved implicitly using an ADI method similar to that proposed by Witelski and Bowen (2003). This method used centered spatial differences and backward time differences, and so is also first order accurate in time, second order in space.

2.3.1 The ADI Method

Much of the presentation of this section is taken from Claridge, Levy, and Wong (2011). Consider the conservation law

$$q_t + \nabla \cdot F(q) = 0 \tag{2.10}$$

where the flux F has the form

$$F(q) = f(q)(-a \nabla q + b \nabla \nabla^2 q). \tag{2.11}$$

Both the film and surfactant equations take this form, notably with $b = 0$ for the surfactant equation. Let q^n be the computed solution at the nth time step. The backwards Euler method takes the form

$$0 = q^{n+1} - q^n + \Delta t \nabla \cdot F(q^{n+1}) = N(q^{n+1}). \tag{2.12}$$

Let δ^n be the update at the nth time step, $\delta^n = q^{n+1} - q^n$. Newton's method applied to Equation 2.12 would require solving

$$N'(q^n)\delta^n = -N(q^n),$$

which is inconvenient because the data q^n is two dimensional. The motivating idea of the ADI method is to factor the operator N' into a product

of two operators $L_x(q)$ and $L_y(q)$, each of which acts only in one spatial dimension. This factorization is given by

$$N'(q) \approx (I + \Delta t \partial_x G_x(q))(I + \Delta t \partial_y G_y(q)) = L_x(q) L_y(q) \tag{2.13}$$

where

$$G_x(q) = f'(q)(-aq_x + b(\nabla^2 q)_x) + f(q)(-a\partial_x + b\partial_{xxx}) \tag{2.14}$$

and G_y is defined analogously in the y-direction.The error incurred in performing the approximate factorization is of order $O(\Delta t^2)$ (Witelski and Bowen, 2003). The application of Newton's method is given by solving the equations

$$\begin{aligned} L_x(q^n)v &= -N(q^n), & (2.15)\\ L_y(q^n)\delta^n &= v, & (2.16) \end{aligned}$$

and then updating q as $q^{n+1} = q^n + \delta^n$. Because each operator acts in only one dimension, the update for v can be computed separately for each horizontal slice of the data and similarly with vertical slices for δ^n.

2.3.2 Discretization

All derivatives are approximated using centered differences, and where cell interface values are needed, the average of adjacent cell values is used. For instance, let $w = (w_1, \ldots, w_n)$ be a one-dimensional slice of cell-centered data. $L_x(q)$ is discretized by first discretizing $\partial_x G_x(q)$ with centered differencing,

$$L_x(q) = I + \frac{\Delta t}{\Delta x}\left(G_x(q)E_{1/2} - G_x(q)E_{-1/2}\right), \tag{2.17}$$

where E is the shift operator; that is, $(E_j w)_i = w_{i+j}$. Values at half-grid points are approximated as $w_{i+1/2} = \frac{1}{2}(w_i + w_{i+1})$, and boundary values are to be noted in the next section. The ith component of $G_x(q)w$ is a centered-difference approximation to Equation 2.14 at cell i, and so

$$\begin{aligned} (G_x(q)w)_i &= \left(f'(q)(-aq_x + b(\nabla^2 q)_x)\right)_i w_i \\ &+ f(q)_i \left(-a\frac{w_{i+1/2} - w_{i-1/2}}{\Delta x}\right) \\ &+ f(q)_i \left(b\frac{w_{i+3/2} - 3w_{i+1/2} + 3w_{i-1/2} - w_{i-3/2}}{\Delta x^3}\right). \end{aligned} \tag{2.18}$$

Note that the operators $G_x(q)E_{\pm 1/2}$ return data evaluated at the interfaces $i \pm 1/2$ in Equation 2.17. As an example of a computation for $L_x(q)$, the value in the ith position of the diagonal of $L_x(q)$ is

$$\begin{aligned} 1 \quad &+ \quad \frac{\Delta t}{\Delta x}\left(\frac{1}{2}C_{i+1/2} + f(q)_{i+1/2}\left(-\frac{a}{\Delta x} + \frac{3b}{\Delta x^3}\right)\right) \\ &+ \quad \frac{\Delta t}{\Delta x}\left(\frac{1}{2}C_{i-1/2} + f(q)_{i-1/2}\left(\frac{a}{\Delta x} - \frac{3b}{\Delta x^3}\right)\right), \end{aligned}$$

where $C_{i+1/2} = (f'(q)(-aq_x + b(\nabla^2 q)_x))_{i+1/2}$. The formulas change somewhat at the boundaries, where indices outside the range of the data are drawn from extrapolation, hence altering the derivative operators. For instance, the first derivative of h at the left boundary is approximated as $\frac{1}{\Delta x}(h_0 - h_1)$ but $h_0 = h_1$ according to the boundary condition $h_x = 0$.

2.4 Efficiency of the Method

The matrices to be solved in Equation 2.15 and 2.16 are banded, with a width of five for the film equation and a width of three for the surfactant equation (for which there is no fourth-order term). Each solve for a slice of data can therefore be completed in a time linear in the length of that data, so for example, with an $m \times n$ grid the solve in Equation 2.15 will require $nO(m)$ steps and the solve in Equation 2.16 will require $mO(n)$ steps. The ADI method can be conveniently parallelized since the one-dimensional solves along each slice of the data are independent of each others. The code is parallelized using the openMP framework.

Chapter 3

Testing the Solver

To verify the solver's accuracy, I have considered several thin film problems for which numerical studies have already been conducted. I have focused on reproducing results for fingering in the case of a thin film on an incline and droplet spreading due to surfactants. Previous results considered here have also been computed numerically using similar ADI methods to the one used here. Considering a thin film problem with surface tension gradients is useful in testing the solver because those effects introduce hyperbolic terms into the equations, so the solver in full (hyperbolic and parabolic parts) can be tested.

3.1 The Porous Medium Equation

A simple but useful application of the solver is to the porous medium equation (PME), defined by

$$u_t = \nabla \cdot \left(g'(u) \nabla h \right)$$

where $g(h) = h^m$ for some integer m. The porous medium equation is a well-studied equation with solutions that the solver should be able to reproduce. Equation 1.30 for the film height in the surfactant spreading can be reduced to the form of the porous medium equation by taking $\kappa = 0$ and $\Gamma = 0$, which becomes

$$h_t = \nabla \cdot \left(\frac{1}{3} h^3 \nabla h \right).$$

This is the equation that describes a thin film relaxing under the force of gravity, with no other effects.

One well-known solution to the porous medium equation is the ZKB solution, which is an axisymmetric similarity solution with compact support. The ZKB solution for Equation 3.1 is given in two dimensions by

$$h(r,t) = t^{-1/4}\left(C - \frac{9}{16}r^2t^{-1/4}\right)_+^{1/3}$$

where C is some constant and $(x)_+ = \max\{x, 0\}$ (Vasquez, 2007). Simulations for this equation were run in two dimensions using initial time $t_0 = 1$ and the initial condition

$$h(x,t_0) = \left(1 - \frac{9}{16}r^2t\right)_+^{1/3}.$$

Figure 3.1 shows a radial slice of the solution at the initial time $t_0 = 1$ and final time $t_0 = 21$, in which it can be seen that the numerical results agree very well with the computed solution. There is a slight discrepancy near the leading edge of the film, the error of which is on the order of the grid spacing (about 0.05). This provides some validation for the solver in handling the gravity-driven spreading term in the surfactant spreading problem, notably with a solution that has compact support and a relatively sharp leading edge.

3.2 Reproducing Fingering

Fingering instabilities arise in a system when a solution is unstable to perturbations transverse to its direction of propagation. If a wave front is perturbed by a periodic disturbance in the transverse direction, those disturbances move faster than the front itself, growing into finger-like shapes. Fingering provides a useful test for the solver because it is dependent on interactions involving the fourth order term of the thin film equation and is an essentially two-dimensional effect. If the solver shows fingering where expected that suggests the solver is computing solutions correctly.

3.2.1 Fingering for a Film on an Incline

One thin film problem in which fingering arises is that of a thin film on an incline driven by a temperature gradient. The temperature gradient is imposed to produce a surface tension gradient in the film that drives the

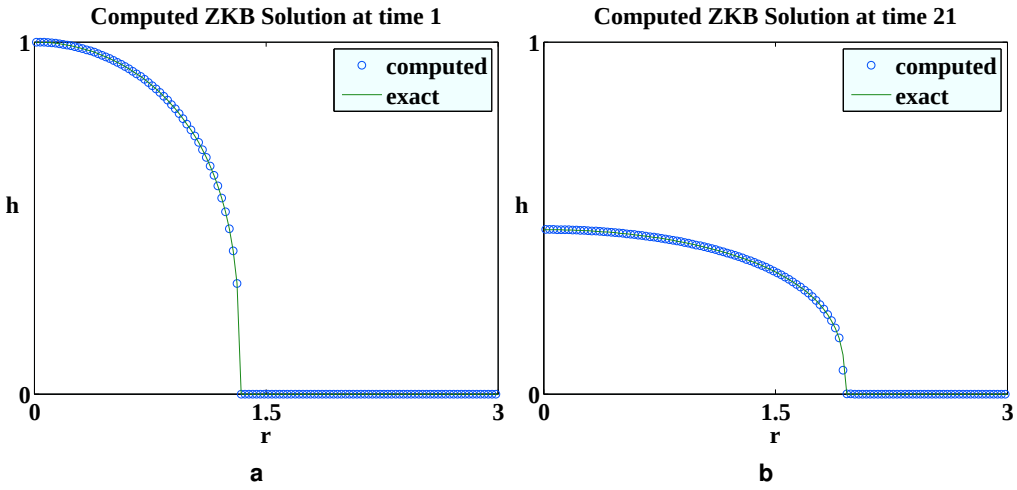

Figure 3.1 Numerical solution of the porous medium equation (Equation 3.1). A radial slice is shown at initial time $t_0 = 1$ (a) and final time $t_0 = 21$ (b), with points representing the numerical solution and solid line showing the exact solution.

flow against gravity, along the incline. The governing equation for the film height is

$$h_t + (h^2 - h^3)_x = \kappa \nabla \cdot (\frac{1}{3} h^3 \nabla \nabla^2 h),$$

where the temperature gradient is imposed in the x-direction. The height is assumed to be constant along the transverse direction, so the problem is one dimensional. Due to the hyperbolic term of the equation, $(h^2 - h^3)_x$, there are compressive wave solutions to this equation. Under certain conditions, compressive waves are unstable to transverse perturbations, which leads to fingering instabilities. Fingering can be induced in a numerical simulation by taking a compressive wave solution and perturbing it by a sine wave of some frequency in the transverse direction. Figure 3.2a shows an example of fingering computed by the numerical solver. The traveling wave solution, which is a single compressive wave, was evolved using the initial condition

$$h(x,0) = \begin{cases} h_L & x < 0 \\ h_L - (h_L - h_R)x^{10} & 0 < x < 1 \\ h_R & x > 1 \end{cases}$$

in the domain $[-10, 160]$ for 120 units of time, enough for it to reach a steady (traveling) state. The perturbation was achieved by taking traveling wave solution $\overline{h}(x)$ and using initial condition

$$h(x, y, 0) = \overline{h}(x + \epsilon \cos(2\pi y/\lambda), 0).$$

The parameters for the simulation presented are $\Delta x = 0.002, \Delta y = \lambda/100$ with a domain of $[0, 50] \times [0, 2\lambda]$ and no-flux boundary conditions in the y direction. The wavelength was chosen as $\lambda = 1.12$, half the y-width of the domain. While the boundary conditions are not periodic, the periodicity of the initial data ensures that the data is periodic for all time. There is some differences between using no flux and periodic boundary conditions for solver, but periodic boundary conditions have not yet been implemented.

These results are largely consistent with the result from Sur, Witelski, and Behringer (2004), shown for comparison in Figure 3.2b. While the qualitative shape of the fingers are in clear agreement, the steady-state finger length is noticeably longer for our solver compared to Sur's results. The steady state length noted by Sur is about 1.4, whereas it is at least 2 here.

3.2.2 Fingering for Surfactant Spreading

To further verify the code for the full surfactant spreading equations, I have reproduced the results of Warner et al. (2004) for fingering in the case of a droplet with surfactant spreading over a thin precursor layer of the same fluid. This model is significantly more complicated than the temperature-driven film in Section 3.2.1 because the surfactant also has an evolution equation of its own, leading to a system of two coupled equations. The model differs from that for the spreading experiment in Section 1.3 in that the film is not initially constant and does not have axisymmetric geometry; however, the governing equations are the same. In Warner's work, an ADI method was also employed to solve the fourth-order term in the equations. However the parabolic term of the surfactant equation Equation 2.9 is treated explicitly there whereas it is treated implicitly in this work (Claridge et al., 2011).

The equations being solved are the surfactant spreading equations Equation 1.30 and Equation 1.31, with parameters $\kappa = \delta = 10^{-4}$, $\beta = 0$ and a linear equation of state. The initial droplet is perturbed using a transverse perturbation that is a combination of wavelengths,

$$h_0(x, y) = h_{drop}(x) + \sum_{i=1}^{N} \cos(ky),$$

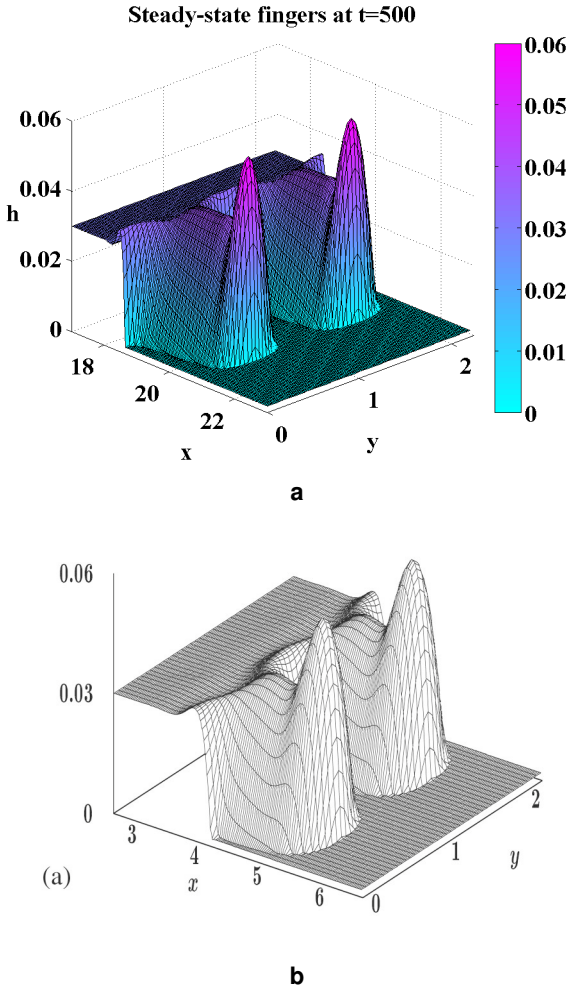

Figure 3.2 Comparison of finger formation from the solver described here (a) and the result from Sur et al. (2004) (b).

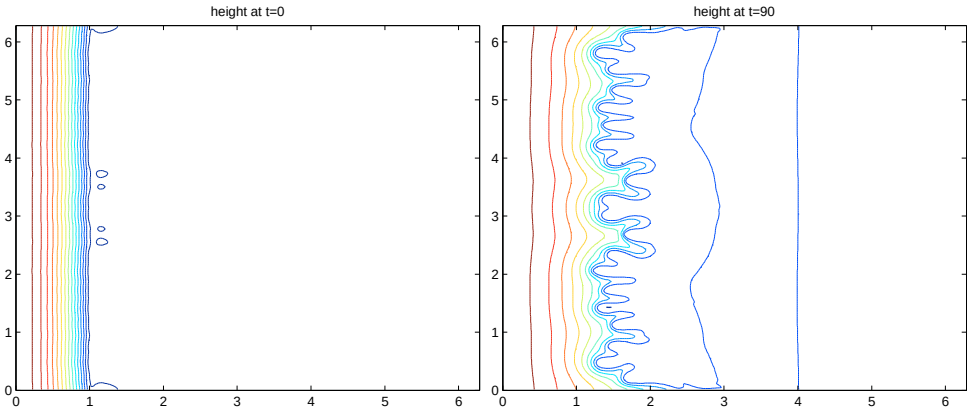

Figure 3.3 Evolution of fingers for a surfactant-laden droplet, reproducing the result from Warner et al. (2004) with good qualitative agreement. Contours show a difference of $1/15$.

where h_{drop} is the unperturbed droplet profile. Our results show good qualitative agreement, with the fingers evolving in the same pattern as described by Warner et al. (2004). The fingering pattern is similar in shape and evolves at the same speed. However, the solver does fail at a late time, $t = 99.2$, which is most likely due to difficulty in computing the solution in the thinning region where fingering occurs; some adjustment to the scheme may be necessary in order to resolve the very small heights that exist there.

It should be noted that while periodic boundary conditions were imposed in in the y-direction, no-flux boundary conditions were used in this simulation. This, however, has little impact on the solution because the initial condition is itself periodic. Also, there is an inconsistency between the solutions in that our results are shifted in the y-direction by π.

3.3 Notes on Time Steps

It is convenient to know, approximately, what time step is required for a given grid spacing to have the ADI method converge (the hyperbolic solver is in most if not all cases less demanding). As a note, the time step can be relaxed after early times, so the "required" time step described here refers to the maximum feasible fixed time step. Simple adaptive time stepping, which halves the time step if the solver fails to converge at the current time step, is currently being used. For outward spreading, multilayer equation of state, $[-5, 5] \times [-5, 5]$ grid, standard coefficient values, the approximate

dx	dt ($\kappa \neq 0, \beta \neq 0$)
0.1	10^{-3}
0.05	2.5×10^{-4}
0.025	5×10^{-7}
0.01	10^{-8}

Table 3.1 Approximate maximum fixed time step usable with a given grid spacing dx.

required time step is summarized in Table 3.1. For comparison, the required time step for $\kappa = 0$ is determined by the hyperbolic part of the system—for instance, about 5×10^{-4} for $dx = 0.01$. It is clear from the table that the κ term makes a dramatic difference, though the 10^{-8} time step suggests something might be wrong.

It is not currently clear whether some inherent stiffness or inefficiency of the solver may be at fault, but regardless the problem suggests the solver may require some modification. The requirement on the time step can be loosened somewhat by allowing for more iterations in the Newton ADI method. The previously mentioned simulations were conducted with ten iterations, declaring failure if convergence was not obtained after that point. Extending the maximum iterations to an excessively large number such as 2000 allows a much larger time step to be used: For instance, with $\Delta x = 0.01$ a time step of about 10^{-6} is required for the first few steps, followed by a step of about 10^{-4}, which is reasonable. However, the number of iterations required for convergence is large.

3.3.1 Convergence Studies

To test convergence, I have tested the solver in the case of outward spreading. Standard values were used for coefficients with the multilayer equation of state. Computations were carried out to time $t = 1$. For convergence in the time step, the grid used was $[-5, 5] \times [-5, 5]$ and Δx was fixed as $\Delta x = 0.1$. Denote by Δt_i the sequence of time steps used to compute the solution to time $t = 1$, and let the corresponding solution for the film height and surfactant at time $t = 1$ be be h_i and Γ_i respectively. The time steps chosen were $\Delta t_i = 2^{-i} \Delta t_0$ for $i \leq 4$ with $\Delta t_0 = 10^{-4}$. Interpreting h_i as a vector of data, denote by $||h_i||$ the ℓ^2 norm. The ratios of differences

given by

$$\frac{||h_{i+1} - h_i||}{||h_i - h_{i-1}||} \tag{3.1}$$

were computed. The ratios in Equation 3.1 were $0.4991, 0.4878$, and 0.5067, for $i = 1, 2, 3$ with similar values for Γ_i, which verifies that the method is first order in time.

Chapter 4

Results for Spreading

In this section, the solver is applied to the model for the experiment described in Section 1.3. For this experiment, the initial film height is constant and surfactant is deposited either within a ring (outward spreading) or outside it (inward spreading). While the full equations are intractable analytically, simplification by neglecting higher order terms leads to similarity solutions that determine the spreading rates and general shape of solutions. The solver provides a way to explore the full equations numerically, although results so far have not shown a way within the existing model to explain the lack of inward spreading.

4.1 Spreading for the Simplified Equations

As motivated by the nondimensionalization of Section 1.5, the most significant term, at least in magnitude, of the film and surfactant equations are the Marangoni terms containing the surface tension gradient $\nabla\sigma$. Setting the gravity-driven spreading, capillarity, and surface diffusion terms to be zero (by setting $\beta = \kappa = \delta = 0$) gives the simplified system

$$h_t + \nabla \cdot \left(\frac{1}{2}h^2\nabla\sigma\right) = 0 \tag{4.1}$$

$$\Gamma_t + \nabla \cdot (h\Gamma\nabla\sigma) = 0. \tag{4.2}$$

Jensen studied this system and found a variety of similarity solutions for both inward and outward spreading (Jensen, 1994), which were verified through (one-dimensional) numerical simulations. Unlike the full equations, the simplified system admits tractable solutions and is therefore useful for validating our numerical solver.

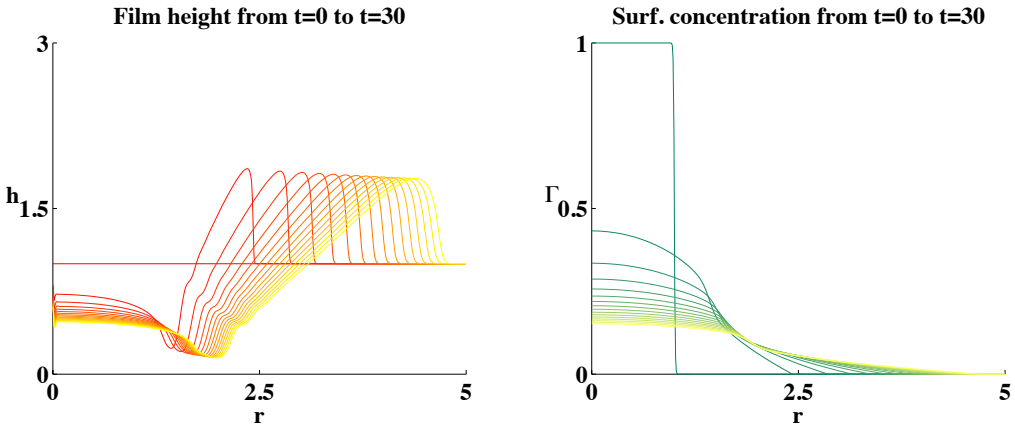

Figure 4.1 Evolution of the film (left) and surfactant (right) profiles for outward spreading with $\beta = \kappa = 0$ and a linear equation of state.

4.1.1 Linear Equation of State

Equations of state can be composed for both outward and inward spreading.

Outward Spreading

For outward spreading, simulations were run with a linear equation of state and the initial condition

$$h(r) = 1, \qquad \Gamma(r) = \frac{m}{2}\left(1 - \tanh(100(r-1))\right) \tag{4.3}$$

with $m = 1$. The results appear to be consistent with Jensen's, notably with the expected spreading rate $r_0(t) \sim t^{1/4}$ for the leading edge of the surfactant.

Inward Spreading

For inward spreading, a linear equation of state was used with the initial condition

$$h(r) = 1, \qquad \Gamma(r) = \frac{m}{2}\left(\tanh(100(r-1))\right) \tag{4.4}$$

and $m = 1$, which approximates a monolayer of surfactant outside the ring $r = 1$. Simulations were run with $\Delta x = \Delta y = 0.01$ in order to resolve the

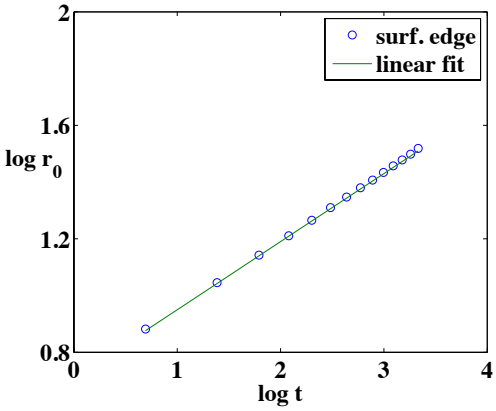

Figure 4.2 Rate of spreading for the position r_0 of the surfactant leading edge, compared to the theoretical prediction of $r_0(t) \sim t^{1/4}$.

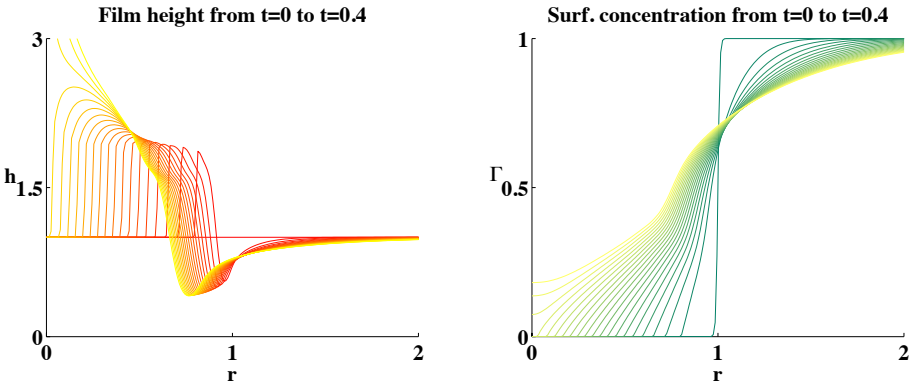

Figure 4.3 Inward spreading with $\beta = \kappa = 0$ and $\delta = 10^{-3}$, until the anti-disk is closed, to reproduce results from Jensen (1994).

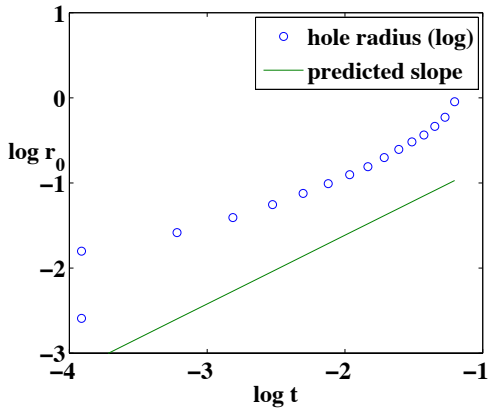

Figure 4.4 Comparison for the inward spreading solution shown in Figure 4.3 of the inner anti-disk radius $r_0(t) \sim (t_0 - t)^\delta$ with $\delta \approx 0.8074$.

shock in the solution. As expected, the surfactant spreads inward, reaching the center of the anti-disk at approximately $t_0 \approx 0.35$. The inner radius $r_0(t)$ of the anti-disk is plotted in Figure 4.4, which evolves roughly as $r_0(t) \sim (t_0 - t)^\delta$ where $\delta \approx 0.8047$, which agrees reasonably well with the theoretical prediction of $\delta \approx 0.804$ from Jensen's similarity analysis. The inward wave in the film height grows to slightly above a height of 2. There is an apparent discrepancy between the closing time, which in Jensen's simulations is $t_0 \approx 1.3$, which has not been resolved.

4.1.2 Multilayer Equation of State

For both inward and outward spreading, using the multilayer equation of state and initial condition Equation 4.4 or Equation 4.3 yields results qualitatively similar to the linear case, for $m = 2$.

4.1.3 Test Equation of State

It would be convenient to be able to explore the effects of the equation of state on solutions. However, for the test equation of state, the solver does not behave as expected. It should be noted that for the full equations, the parabolic solver cannot integrate the equations, most likely due to the large gradients in the problem.

Investigating outward spreading with initial condition Equation 4.3 and $m = 2$ but with the test equation of state Equation 1.38 yields some surpris-

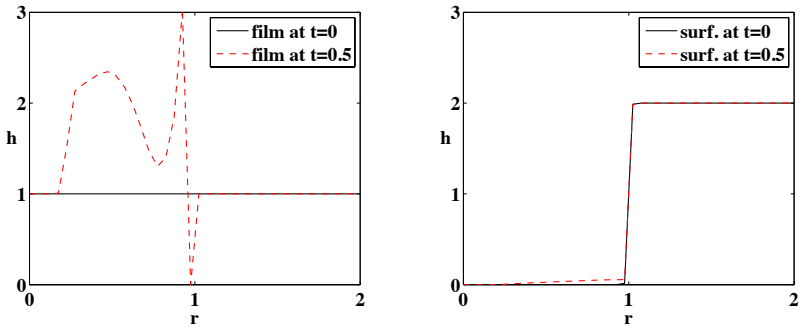

Figure 4.5 Profile of the film (left) and surfactant (right) for inward spreading with test equation of state and $\beta = \kappa = 0$ at times $t = 0$ and $t = 0.5$. The surfactant profile is almost stationary, and the film has an inward-moving wave as well as a sharp bump near $r = 1$.

ing results. The surfactant profile does not move except some spreading that occurs with Γ small, with spreading consistent with the predicted exponent $\delta \approx 0.8047$. Fluid appears to be driven in an outward direction, continuously decreasing the film height near $r = 1$ until it reaches zero. This results in an outward moving wave connected by a rarefaction of sorts to $r = 1$, where there is a shock with $h = 0$ as an endpoint. Obviously, this solution is not of physical relevance, at the very least because the film reaches a height of 0. This solution is shown at times $t = 0$ and $t = 0.5$ in Figure 4.5. At $t = 0.5$, the inward moving wave in the film has formed and nearly reached the center. The surfactant is mostly static, with a very small amount diffusing inward. It appears that the film wave that evolves does so to the left of $r = 1$, where there is little surfactant, and so there is almost no surfactant transported inward.

To clarify the evolution of the surfactant, a smoother initial condition was used, $\Gamma(r) = \frac{m}{2}(1 + \tanh(4(r-1))$. The results are shown in Figure 4.6 and are qualitatively similar, though the spreading inward of the surfactant is more clear. Notable is the vertical portion of the profile. The maximum height at which surfactant spreads is related to the sharpness of the profile shape.

4.2 Spreading for the Full Equations

Adding the gravity (β) and capillary (κ) terms to the simplified equations smooths the solutions. The essential behavior of the system is expected to

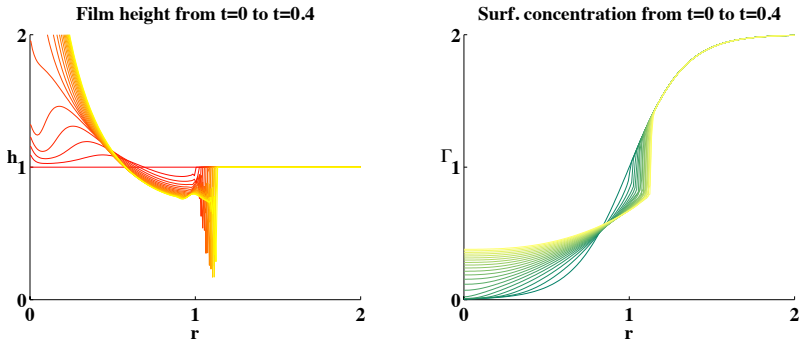

Figure 4.6 Evolution of the film (left) and surfactant (right) profiles for inward spreading using the test equation of state, two monolayers of surfactant and a shallow initial condition $\Gamma(r,0) = \frac{1}{2}(1+\tanh(4(r-1))$. The expected surfactant spreading occurs only within a certain range of r because of the lack of a surface tension gradient for $\Gamma > 1$.

be governed by the Marangoni terms (Peterson, 2010). Numerically, the smoothing of solutions should make computation somewhat less difficult as large gradients and shocks are smoothed. For the most part, applying the numerical solver to the full equations confirm these predictions. Qualitative behavior of the system—spreading rates and the general shape of propagating waves—are the same as for Section 4.1. However, for the test equation of state Equation 1.38, the lack of spreading found in the simple case is not seen for the full equations.

4.2.1 Multilayer Equation of State

The numerical simulations for outward spreading, using the initial conditions (Equation 1.33), appear to agree reasonably well qualitatively with the experimental results of Fallest et al. (2010). Figure 4.7 shows numerical simulations of Equations 1.30 and 1.31 modeling the evolution of film and surfactant. The height profile exhibits an outward spreading front. The surfactant spreads outward with the leading edge approximately at the position of the maximum in the spreading front of the film. This spreading occurs at a rate of $t^{1/4}$, as predicted by similarity solutions in the simplified case in Section 4.1. The height profile includes an outward moving wave that propagates and then spreads with the surfactant front, as well as an inward moving wave that relaxes, again consistent with experiment.

For inward spreading, surfactant is placed outside rather than inside the ring. The experiments for inward spreading (Daniels et al. (2010)) show

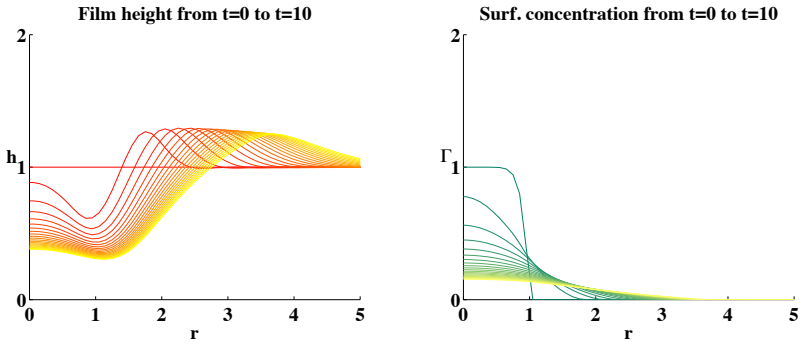

Figure 4.7 Evolution of the film (left) and surfactant (right) profiles for outward spreading, from numerical simulations. For the film, the gradient from red to yellow indicates increasing time, and green to yellow for the surfactant. The domain used is $[-8,8] \times [-8,8]$ in order to ensure the outer boundary conditions did not significantly affect to the solution.

the novel result of a surfactant profile that does not spread with time. This result does not agree with the results of the model using the equation of state Equation 1.37 and initial conditions from Equation 1.34, which exhibits spreading of the surfactant. It is suspected that the experimental results require better resolution or there is a force balance keeping the surfactant static that may not be reflected in the model.

It is possible that an equation of state such as σ_{test} with $\sigma' = 0$ could change the character of solutions enough to produce such behavior. It also may be important to consider initial surfactant profiles with more than one monolayer, $\Gamma \gg 1$. In the experiments cited, $\Gamma \approx 30$ for outward and $\Gamma \approx 5$ for inward spreading, which could differ significantly from monolayer spreading. It should be noted that inward spreading may still be occurring as well, but at a low level, below the threshold for detection in the noted experiments. The next section describes some of the problems that have arisen in trying to compute solutions of the model with the new equation of state, or with large surfactant concentrations.

4.2.2 Test Equation of State

Currently, Newton's method will not converge for the solver when attempting to integrate the full equations for outward or inward spreading, as briefly discussed in Section 3.3. The source of the problem is not clear, but does not seem to be specific to the test equation of state, since a very small time step is required even for the multilayer equation of state.

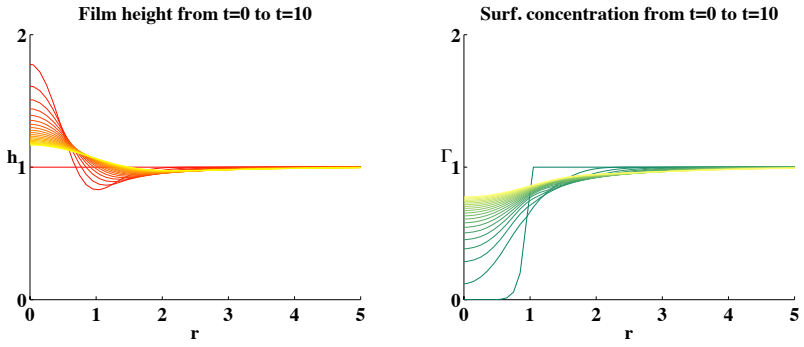

Figure 4.8 Evolution of the film and surfactant profiles for inward spreading, from numerical simulations. The domain and labeling scheme are as in Figure 4.7.

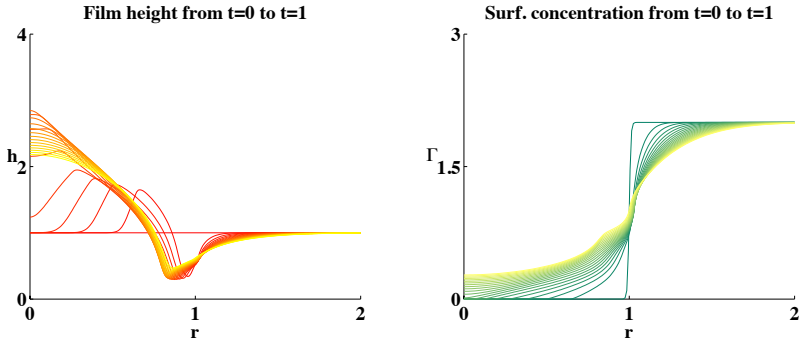

Figure 4.9 Evolution of the film (left) and surfactant (right) profiles for inward spreading using the test equation of state, and $\beta = 0.271$ but $\kappa = 0$. Spreading occurs as expected, in comparison to the case when $\beta = 0$ (Figure 4.5).

If instead κ is set to zero but β is left at the standard value $\beta = 0.271$, the the solver can compute the results. Interestingly, the profile for inward and outward spreading resemble qualitatively the solution for the multilayer equation as in Figure 4.7 and Figure 4.8. In particular, it does not exhibit the lack of spreading as in the simple case, as shown in Figure 4.9.

4.3 Modifications to the Model

The inward spreading that occurs in numerical simulations suggests that the model is inappropriate for the problem. Modification of the equation of state may allow for steady-state solutions to more readily exist, although it

would seem from the aforementioned numerical difficulties that there may be some critical aspect of the physical scenario not captured in the model.

One possible factor to consider in changing the model is the inclusion of a varying surfactant diffusivity in place of the constant δ, so that diffusion is resisted by sufficiently large deposits of surfactant. This has been modeled with an equation of state $D(\Gamma)$ and, with a simplified film-surfactant system in planar geometry, shown to be relevant in the existence of steady states (Borgas and Grotberg, 1988). It is unlikely that this modification will significantly alter solutions given the relative unimportance in the δ term that has been numerically observed, but it still may be worth considering.

The lubrication assumption may also not be accurate. Where the surface tension gradient is large, the "flatness" assumed in lubrication theory may not be applicable, and curvature effects could be important in inhibiting the inward flow of surfactant. The addition of corrections to the curvature may be possible without losing equations for the film height and surfactant, although such corrections might also require abandoning lubrication theory entirely. Although this would have the advantage of making fewer assumptions, it would make computation significantly more difficult.

Chapter 5

Conclusions

A numerical solver for thin film problems has been tested and applied to a problem in surfactant spreading. The solver has been shown to reasonably reproduce results for fingering in the case of a thin film on an incline and for droplet spreading due to surfactant. In applying the solver to the problem of surfactant spreading of a disk, numerical results agree with theoretical solutions found by Jensen. Modifying the equation of state changes the behavior of the system dramatically without regularizing terms ($\beta, \kappa \neq 0$ smooth the solution), producing solutions with limited spreading. However, these results still do not agree with the nonspreading solutions found experimentally. There are several directions in which this research can be continued and extended.

Of primary importance is a resolution of the numerical difficulties apparent in the solver. The small time steps noted in Section 3.3 suggest that some improvements to the solver may be necessary in order to make computations on refined grids feasible. In some cases, stiffness may be an issue that needs to be addressed; the convergence of the Newton ADI method currently appears to be fairly slow. A more careful comparison of methods, especially different choices of splitting between implicit and explicit terms, remains to be done (although partly completed in consideration of the work of Warner et al. (2004) on droplet spreading).

The experimental inward spreading results suggest the model may need to be revised; we hope to devise a better model that will be able to predict this behavior. One possible change to explore is a variation of the equation of state in order to produce fundamentally different solutions than those the model currently produces, although simply modifying the equation of state does not appear thus far to change behavior in the correct way. The

limited spreading solutions in Section 4.2.2 are interesting but require further exploration to see if they are of any relevance. A lack of spreading may also be able to be found in a modified model that takes into account other factors. For instance, the surfactant itself can be considered as more than simply a concentration on the surface; micelle formation or other structural considerations of the surfactant deposit could significantly change the behavior of the system. It is also possible that lubrication at least partly fails for the system, especially considering the meniscus that forms in experiments; A nonlubrication model, would, however, require implementation of a very different kind of solver (one suited to the full Navier-Stokes equations rather than a reduced equation for the film boundary).

This work is part of an ongoing collaboration between Harvey Mudd College, Duke University, North Carolina State University, and University of Washington. Further research into the dynamics of surfactant spreading will continue during the summer of 2011, both through physical experiments and further numerics.

Bibliography

Allison, Kali, Wynn Vonnegut, and Karen Daniels. 2010. The inward spreading of a thin film of insoluble surfactant. NSF DMS-0604047.

Borgas, Michael S., and J.B. Grotberg. 1988. Monolayer flow on a thin film. *J Fluid Mech* 193:154–170.

Bull, J.J., and J.B. Grotberg. 2003. Surfactant spreading on thin viscous films: Film thickness evolution and periodic wall stretch. *Experiments in Fluids* 34:1–15.

Claridge, Jonathan, Rachel Levy, and Jeffrey Wong. 2011. Finite volume methods for nonlinear systems modeling thin films and surfactants. *preprint* .

Craster, R.V., and Omar K. Matar. 2000. Surfactant transport on mucus films. *Journal of Fluid Mechanics* 425:235–258.

Daniels, Karen, Kali Allison, Jonathan Claridge, Rachel Levy, Ellen Peterson, Michael Shearer, Wynn Vonnegut, and Jeffrey Wong. 2010. The dynamics of droplets and holes in thin surfactant films. In *APS Division of Fluid Dynamics*.

Edmonstone, B.D., R.V. Craster, and Omar K. Matar. 2006. Surfactant-induced fingering phenomena beyond the critical micelle concentration. *J Fluid Mech* 510:105–138.

Fallest, David W., A.M. Lichtenberger, C.J. Fox, and Karen Daniels. 2010. Fluorescent visualizations of a spreading surfactant. *New J Phys* .

Jensen, O.E. 1994. Self-similar, surfactant-driven flows. *Physics of Fluids* 6:1084–1094.

Leveque, Randall. 2002. *Finite Volume Methods for Hyperbolic Problems*. Cambridge University Press.

Leveque, Randall J., and M.J. Berger. 2010. CLAWPACK v.4.5.0. URL http://www.clawpack.org.

Peterson, Ellen. 2010. *Flow of Thin Liquid Films with Surfactant: Analysis, Numerics, and Experiment.* Ph.D. thesis, North Carolina State University.

Sur, J., T.P. Witelski, and R. P. Behringer. 2004. Steady-profile fingering flows in Marangoni driven thin films. *Physical Review Letters* 93.

Vasquez, Juan Luis. 2007. *The Porous Medium Equation: Mathematical Theory*. Oxford University Press.

Warner, M.R.E., R.V. Craster, and Omar K. Matar. 2004. Fingering phenomena associated with insoluble surfactant spreading on thin liquid films. *J Fluid Mech* 510:169–200.

Witelski, Thomas P., and Mark Bowen. 2003. ADI schemes for higher-order nonlinear diffusion equations. *Applied Numerical Mathematics* 45(2-3):331–351.